European Journal of Radiology 117 (2019) 41–48

Contents lists available at ScienceDirect

European Journal of Radiology

journal homepage: www.elsevier.com/locate/ejrad

Multimodal magnetic resonance imaging of peripheral nerves: Establishment and validation of brachial and lumbosacral plexi measurements in 163 healthy subjects*

Xiaoyun Su[a,b], Xiangquan Kong[a,b], Dingxi Liu[a,b], Xiangchuang Kong[a,b], Osamah Alwalid[a,b], Jing Wang[a,b], Shenglei Shu[a,b], Chuansheng Zheng[a,b,*]

[a] Department of Radiology, Union Hospital, Tongji Medical College, Huazhong University of Science and Technology, Wuhan, 430022, China
[b] Hubei Province Key Laboratory of Molecular Imaging, Wuhan, 430022, China

ARTICLE INFO

Keywords:
Magnetic resonance neurography
Brachial plexus
Lumbosacral plexus
Contrast-enhanced
Diffusion tensor imaging

ABSTRACT

Purpose: This study aims to provide normal reference values for quantitative parameters for brachial and lumbosacral plexi on multimodal MRI. In addition, the parameter variations between the left and right sides, the individual nerve groups, genders and age groups were also evaluated.

Materials and methods: Multimodal MRI was evaluated in 163 healthy subjects, who were randomly divided into three groups: brachial plexus, lumbosacral plexus and diffusion tensor imaging groups. Nerve diameters, contrast ratios, T2 nerve-muscle signal ratios (nT2), fractional anisotropy (FA) values and apparent diffusion coefficients (ADC) were measured in both plexi. Parametric tests and Pearson correlation for normally distributed data, and non-parametric tests and Spearman correlation for non-normally distributed data were used.

Results: There were no significant differences in parameters between the left and right sides. The diameters of the C7, L4-S1, sciatic, and femoral nerve roots were larger in men than in women ($P < 0.05$). The nT2 in the brachial and lumbosacral plexi and the contrast ratio in the lumbosacral plexus were significantly higher in the elderly. The diameter of the S1 nerve root was smaller in the elderly. There were no significant differences between the individual nerve groups in contrast ratios and in brachial plexus nT2. A gradual increase in the nT2 from the top to the bottom was observed in the L4-S1 nerve roots ($P < 0.05$).

Conclusion: This study provides multi-parameter normative data for the brachial and lumbosacral plexi while considering differences between the two sides, the individual nerves, genders, and the ages.

1. Introduction

MR neurography has become an effective tool for investigating the peripheral neuropathies, such as trauma, entrapment and inflammatory disorders [1]. The three-dimensional (3D) sampling perfection with application-optimized contrasts using different flip-angle evolutions (SPACE) and the short time inversion recovery (STIR) sequences allow for the visualization of the peripheral nerves [2–5]. The commonly used parameters for assessing peripheral nerves include the diameter or the cross-sectional areas of the nerve roots, the T2 nerve signal values, and the fractional anisotropy (FA) values [6–8]. Previous studies have demonstrated that Wallerian degeneration and demyelination led to partial or diffuse thickening and increased T2 signal intensity [9,10]. These characteristics of the pathologic changes promote structural visualization and quantitative analyses. Such visualization and analyses are helpful not only for disease diagnosis, but also for monitoring regeneration and treatment responses. To the best of our knowledge, there are only a few studies that have quantitatively measured the

Abbreviations: 3-D, three-dimensional; ADC, apparent diffusion coefficient; CE, contrast-enhanced; CR, contrast ratio; DRG, dorsal root ganglion; DTI, diffusion tensor imaging; FA, fractional anisotropy; LS, lumbosacral; MIP, maximum intensity projection; nT2, T2 nerve-muscle signal ratio; SPACE, sampling perfection with application-optimized contrasts using different flip-angle evolutions; STIR, short time inversion recovery; TIRM, turbo inversion recovery magnitude; VIBE, volumetric interpolated breath-hold examination

* **Work originated:** Department of Radiology, Union Hospital, No. 1277 Jiefang Avenue, Wuhan City, Hubei Province, China.
* Corresponding author at: Department of Radiology, Union Hospital, Tongji Medical College, Huazhong University of Science and Technology, Wuhan, 430022, China.
E-mail addresses: nhsuxiaoyun@163.com (X. Su), kxq0525@126.com (X. Kong), 462790783@qq.com (D. Liu), hongke80@163.com (X. Kong), Dr.osamah_alwalid@yahoo.com (O. Alwalid), jjwinflower@126.com (J. Wang), shusl1992@163.com (S. Shu), whxhchuansheng@126.com (C. Zheng).

https://doi.org/10.1016/j.ejrad.2019.05.017
Received 27 February 2019; Received in revised form 19 May 2019; Accepted 23 May 2019

structural MR properties of peripheral nerves [10–15], and there are even fewer studies that evaluate the multimodal parameters of the brachial and lumbosacral (LS) plexi in healthy subjects.

This study aims to provide normal reference values for the C5-C8 and L4-S1 nerve roots, including the diameter, contrast ratio (CR), T2 nerve-muscle signal ratio (nT2), FA, and apparent diffusion coefficient (ADC). In addition, the parameter differences between the left and right sides, the individual nerve groups, genders and ages were also investigated.

2. Materials and methods

2.1. Ethics approval

The present study was approved by the ethics committee of our hospital (No. IORG0003571) and was registered on ClinicalTrials.gov (ChiCTR XX). Written informed consent was obtained from all the subjects.

2.2. Subjects

From October 2017 to November 2018, 163 healthy subjects (79 men and 84 women) were recruited from the staff members of our institution. Their ages ranged from 18 to 65 -year old with the median age at 38. The subjects were divided into two age groups: the young group and the elder group with the age range at 18–40 years and 40 + years, respectively. 97% (158/163) of the subjects are right-handed. All the subjects were asymptomatic, and did not suffer from any diseases and/or receive any drugs that may alter the sensory or motor functions at the time of enrollment. The subjects were randomly divided into three groups: the brachial plexus group (n = 54, 29 men, age = 40.53 ± 13.5 years, body mass index (BMI) = 23.5 ± 0.4 kg/m^2), the LS plexus group (n = 54, 24 men, age = 38.55 ± 10.7 years, BMI = 22.9 ± 0.4 kg/m^2), and the diffusion tensor imaging (DTI) group (n = 55, 26 men, age = 38.40 ± 11.4 years, BMI = 23.1 ± 0.4 kg/m^2). The following exclusion criteria were adopted: history of a metabolic, renal, neurological or neuromuscular disorder, vertebral disc herniation, and/or contraindication(s) to MRI.

2.3. MRI scanning protocol

Subjects were placed on the gantry in the supine position with the head in the neutral position. Brachial plexus examination was performed on a 1.5-T MR scanner (MAGNETOM Aera, Siemens Healthcare, Germany) with the head neck coupling and multichannel body matrix coils from the skull base to the sternal body. LS plexus examination was performed on a 3-T MR scanner (MAGNETOM Trio, Siemens Healthcare, Germany) with two multichannel body matrix coils and six elements of spine array coils. For the LS plexus imaging, MR scanning covered the areas from the level of the superior edge of the T12 vertebra to the upper part of the femur. DTI examination was performed on a 3-T MR scanner and included both the brachial and the LS plexi.

The MRI protocols of the brachial plexi group and the LS plexi group included the turbo inversion recovery magnitude (TIRM), volumetric interpolated breath-hold examination (VIBE), and 3D-SPACE-STIR sequences on the coronal plane. First, TIRM and VIBE sequence plain scans were performed. Then, a contrast agent (Gadovist, Bayer Pharma AG) was administered by an intravenous injection of 0.15 mL/kg and with a flow rate of 1.5 ml/s. Contrast-enhanced (CE)-VIBE and 3D-SPACE-STIR sequence scans were performed after the administration of the contrast agent. The MRI protocols of the DTI group included the single-shot-echo–planar-imaging based DTI sequences on the axial plane. Sequence parameters are given in Table 1.

2.4. Image processing and analysis

Built-in post-processing software (3D Syngo MR workspace, Siemens Healthcare, Erlangen, Germany) was used for the reconstruction of the maximum intensity projection (MIP) images. All the measurements were performed independently by two experienced neuroradiologists and were repeated 3 times; the averaged values were used. The region of interest (ROI) and their corresponding measurements are illustrated in Fig. 1 and supplementary Figure S.1.

2.4.1. Nerve diameters

On the reconstructed MIP 3D-SPACE-STIR images (slice thickness = 15 mm), the diameters of the nerves at the C5-C8 and L4-S1 levels were measured perpendicular to their long axis at 1.0 to 2.0 cm away from the dorsal root ganglion (DRG) on both sides (Fig. 1a). The diameters of the sciatic and femoral nerves on both sides were measured on the coronal and sagittal planes, respectively, at the upper edge of the femoral head.

2.4.2. Contrast ratios

The mean signals of CE-VIBE and non-CE-VIBE were measured for the bilateral C6-C8 and L4-S1 nerve roots at the same location by copying the ROIs between the two sequences (Fig. 1b, c). The contrast ratio was defined as CR = CE-VIBE signal intensity / non-CE-VIBE signal intensity.

2.4.3. T2 nerve-muscle signal ratios

The nT2s were measured on the TIRM sequence images (Fig. 1d). The ROIs were used to measure the T2 signal intensity of the bilateral C6-C8 and L4-S1 nerve roots, and the adjacent deep neck and iliopsoas muscles. The nT2 was defined as nT2 = nerve root T2 signal intensity / adjacent muscle T2 signal intensity.

2.4.4. DTI parameters

The mean FA and ADC values were measured on the DTI sequence images by drawing a circular ROI bilateral on the brachial and LS plexi (Supplementary Fig. 1). The ROIs of C5-C8 and L4-S1 nerve roots were set to beyond 1.0 to 2.0 cm of the DRG on both sides. ROIs of the C6-C7 and L5-S1 DRGs were set at the ganglia. A total of 22 data points (eight ROIs from C5 to C8, six ROIs from L4 to S1, and eight ROIs from the DRG) for each subject were obtained.

The same readers, who were blinded to the initial results, repeated the post-processing and analyses of the images after 8 weeks. The image qualities were evaluated based on the presence and severity of the motion and pulsation artifacts which affect nerve visualization, and were then classified into three grades (1: excellent, 2: fair, 3: poor image quality). Images that were rated as “poor” were excluded.

2.5. Statistical analyses

Statistical analyses were performed using the GraphPad prism 6.0 and the IBM SPSS statistical software version 22 (IBM Corp., Armonk, UY, USA). Normally distributed data were expressed as mean ± standard deviation ($\chi \pm s$). Categorical or nonnormally distributed data were expressed as median (M) and quartiles (P25, P75). The contingency table approach and the Kruskal-Wallis H tests were used to compare the demographic differences (i.e., genders and ages) among the groups. Paired-samples *t*-test (or Wilcoxon signed-rank test) was used to assess the differences of the nerve roots (or ganglia) between the two sides and between the individual nerve groups. Independent-samples *t*-test (or Wilcoxon rank test) was used to compare the nerve roots (or ganglia) between genders and between age groups. Pearson (or Spearman rank) correlation test was used to detect the correlations between the diameters and BMI, between the different DTI parameters, and between the DTI parameters of the nerve roots (or ganglia) and ages. Intraclass correlation coefficients were obtained for interreader

Table 1
Magnetic Resonance Sequence Parameters[a].

	SPACE		VIBE		TIRM		DTI
	3.0T	1.5T	3.0T	1.5T	3.0T	1.5T	3.0T
TR (ms)	3000	3000	8.18	7.04	4000	3830	6000
TE (ms)	270	248	3.04	2.39	39	58	92
Average	1.8	2	1.8	1	2	2	4
Slice	144	120	120	120	37	30	45
FOV (mm)	448 × 448	384 × 384	448 × 448	384 × 384	448 × 448	384 × 384	256 × 256
Voxel (mm^3)	1.0 × 1.0 ×1.0	1.0 × 1.0 ×1.0	1.0 × 1.0 ×1.0	1.0 × 1.0 ×1.0	1.5 × 1.2 ×4.0	1.2 × 1.2 ×3.0	2.0 × 2.0 ×3.0
BW(Hz/px)	425	425	130	560	250	250	1345
Fat saturation	FS + STIR	FS + STIR	SPAIR	Dixon	—	—	FS
Other	IPAT = 3	—	IPAT = 2	IPAT = 2	IPAT = 2	IPAT = 2	B = 0,900 s/mm^2; DOI-20; IPAT = 2,
TA (min)	12'14	11'17	2'40	2'02	4'20	3'47	5'32

TR: repetition time; TE: echo time; TA: acquisition time; FOV: field of view; BW: bandwidth; PX: pixel; FS: frequency selective; STIR: short T1 inversion recovery; SPAIR: spectral adiabatic inversion recovery; B: diffusion moment in s/mm^2; DOI: directions of interrogation; IPAT: integrated parallel acquisition technique; SPACE: sampling perfection with application-optimized contrasts using different flip angle evolution; TIRM: turbo inversion recovery magnitude; VIBE: volumetric interpolated breath-hold examination; DTI: diffusion tensor imaging;

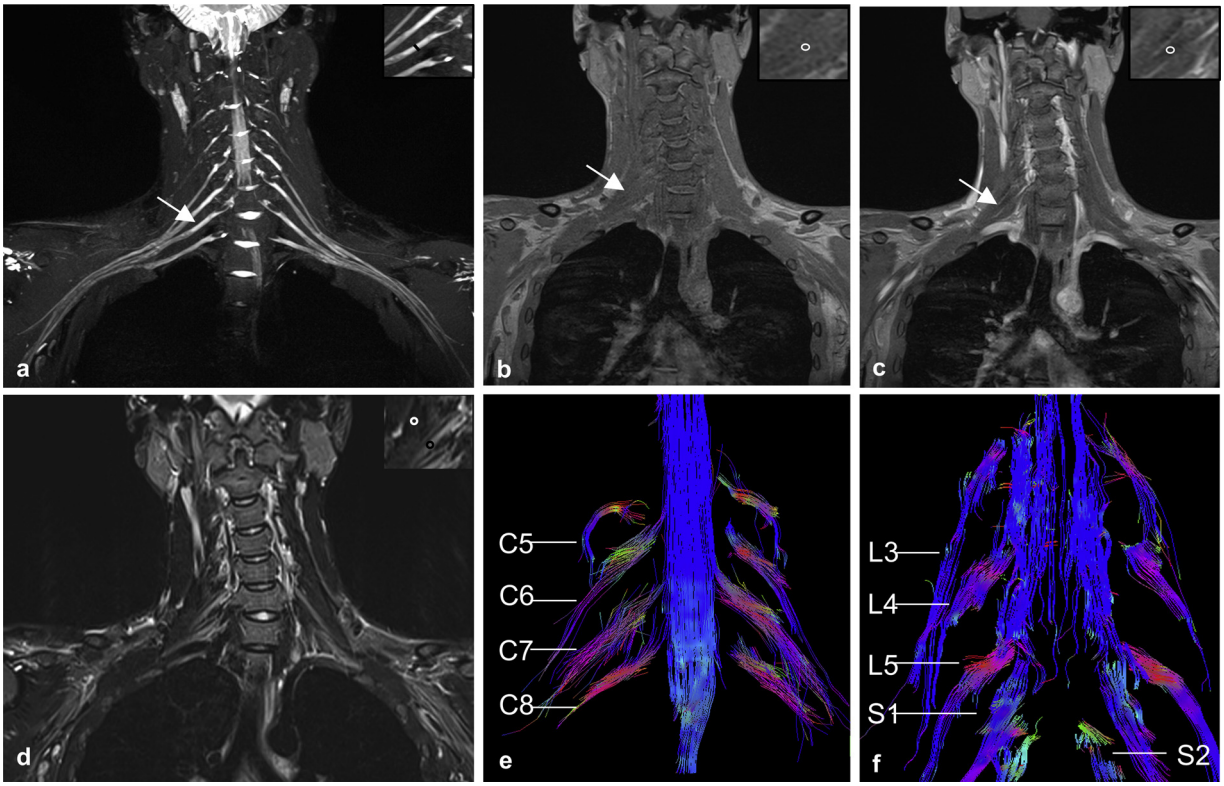

Fig. 1. Coronal reconstructed MIP 3D-SPACE-STIR image of a volunteer (a) showing the whole course of the brachial plexus. The arrow indicates the right C7 nerve root. Images b and c show the right C7 nerve root (arrows) on non-CE-VIBE and CE-VIBE images. The T2 nerve-muscle signal ratios were obtained by selecting a ROI on TIRM sequence images (d). Tractographies (e, f) show treelike configurations and microstructural properties in the brachial and lumbosacral plexi. Magnified views of the areas of interest on the right C7 nerve root and the corresponding measurements (nerve diameter (a), contrast ratio (b, c) and T2 nerve-muscle signal ratio (d)) are shown in the right upper corners of the images.a–d.

and intrareader reliability. $P < 0.05$ was considered statistically significant.

3. Results

3.1. Demographics and quality assessments

There were no significant differences in ages ($\chi^2 = 1.982$, $P = 0.371$) and in genders ($\chi^2 = 1.206$, $P > 0.05$) among the three subject groups. The BMIs of the three groups were normally distributed (Supplementary Figure S.2). There was no significant difference between genders in BMI ($P = 0.81$). Five poor-quality DTI images of the brachial plexus were excluded due to the severe motion artifacts (Supplementary Table 1). The representative images are shown in Figs. 1 and 2. The architectural configurations of the reconstructed fiber bundles C5 to C8 are shown from six different angles (Supplementary Figure S.3).

3.2. Diameters and DTI

The diameters and the FA and ADC values of the nerve roots are shown in Table 2.

3.3. Sides and genders

There were no significant differences between the left and the right

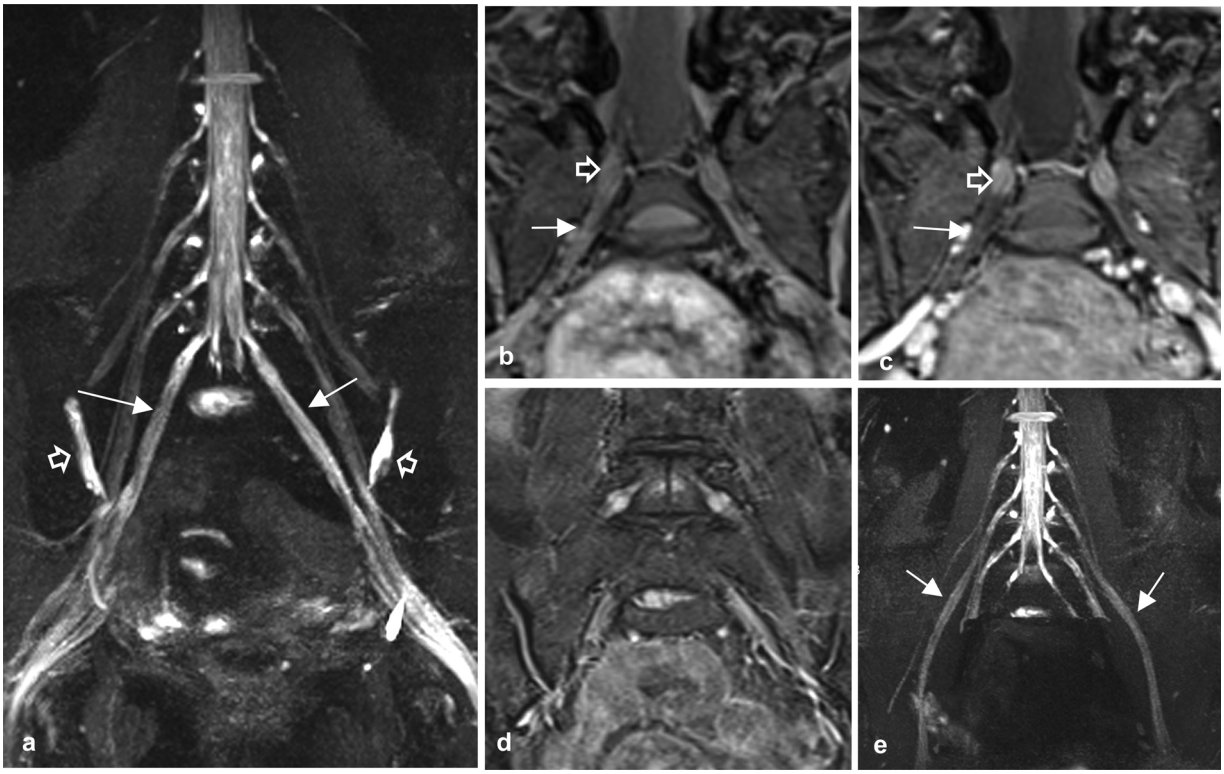

Fig. 2. The diameters of the nerve roots at the S1 (arrows) were measured perpendicular to their long axis on the reconstructed MIP 3D-SPACE-STIR image (a). The patch long T2 signal on both sides shows the effusion of the bilateral sacroiliac joints (hollow arrows). Images b and c show the right S1 nerve roots (arrows) and ganglia (hollow arrows) on non-CE-VIBE and CE-VIBE images. T2 nerve-muscle signal ratios were obtained by selecting ROIs on TIRM sequence images (d). Reconstructed MIP 3D-SPACE-STIR image (e) of a volunteer shows the bilateral femoral nerves (arrows).

Table 2
Diameters and FA &ADC values[a].

	diameter (mm)	FA	ADC
C5	3.74 ± 0.35	0.401 ± 0.06	1.536 ± 0.18
C6	4.57 ± 0.51	0.449 ± 0.07	1.433 ± 0.15
C7	4.86 ± 0.55	0.479 ± 0.08	1.400 ± 0.13
C8	4.19 ± 0.47	0.475 ± 0.07	1.386 ± 0.14
S1	5.27 ± 0.53	0.428 ± 0.07	1.400 ± 0.16
L5	5.99 ± 0.66	0.439 ± 0.06	1.316 ± 0.15
L4	4.86 ± 0.54	0.442 ± 0.07	1.324 ± 0.15
sciatic	9.92 ± 0.99	N/A	N/A
femoral	4.72 ± 0.69	N/A	N/A

FA: fractional anisotropy; ADC: apparent diffusion coefficient ; N/A : Not available.

side of the nerve roots for all the parameters (P range = 0.052 - 0.956; Supplementary Table 2). There was no statistically significant correlation between the diameters and BMI (brachial plexus, $P = 0.87$; LS plexus, $P = 0.13$). The diameters of the C7 and L4-S1 nerve roots and of the sciatic and femoral nerves were larger in men than in women (all $P < 0.05$, Fig. 3b and d). Further analysis revealed that there were no significant differences in the CR, nT2, FA, and ADC values between genders (P range = 0.193 - 0.891; Supplementary Table 2).

3.4. Individual nerves groups

There were significant differences in the diameters between the individual nerve groups ($P < 0.05$), except for the L4 and femoral nerve (Fig. 3a and c). Comparing the CR and nT2 of the individual nerve groups, only the nT2 of the LS plexus showed significant differences (Table 3). The nT2 of the L4-S1 nerve roots were 2.055 ± 0.41, 2.280 ± 0.53, and 2.673 ± 0.59, respectively. A gradual increase in the nT2 values from the top to the bottom was observed, with the S1 nerve root showing the highest T2 signal.

3.5. Age differences and correlations

The diameter of the S1 nerve roots was significantly smaller in the elder group (5.13 ± 0.49 mm) than in the young group (5.37 ± 0.53 mm; $P = 0.022$). The CR at the LS plexus was significantly higher in the elder group ($P = 0.03$, Fig. 4a). The nT2 values at the brachial plexus and the L4-S1 nerve roots were significantly higher in the elder group (P range = 0.002-0.019; Fig. 4b and Supplementary Table 3). A negative weak correlation between the FA value and the ages at the C8 nerve root ($r = -0.25$, $P = 0.011$) was obtained by the Pearson correlation analysis, while no correlations between the FA or ADC values and the ages were obtained at the rest of the nerve roots (Supplementary Table 3).

3.6. DTI parameters correlation

Significant weak negative correlations were observed between the FA and ADC values at the nerve roots of brachial plexus ($r = -0.349$, Fig. 5a) and LS plexus ($r = -0.262$, Fig. 5c). Moderate negative correlation between the FA and ADC values at the ganglia of the brachial plexus (r's = −0.441, Fig. 5b) and LS plexus (r's = −0.428, Fig. 5d) were observed by the Spearman rank correlation analysis.

3.7. DRG

Regarding the ganglia, no significant differences were observed between the left and right sides or between genders (P range = 0.053-0.956, supplementary Table 4). No significant correlation was observed between the ganglia and the ages (P range = 0.078 - 0.886; Supplementary Table 5). The FA of the ganglia at the brachial and LS

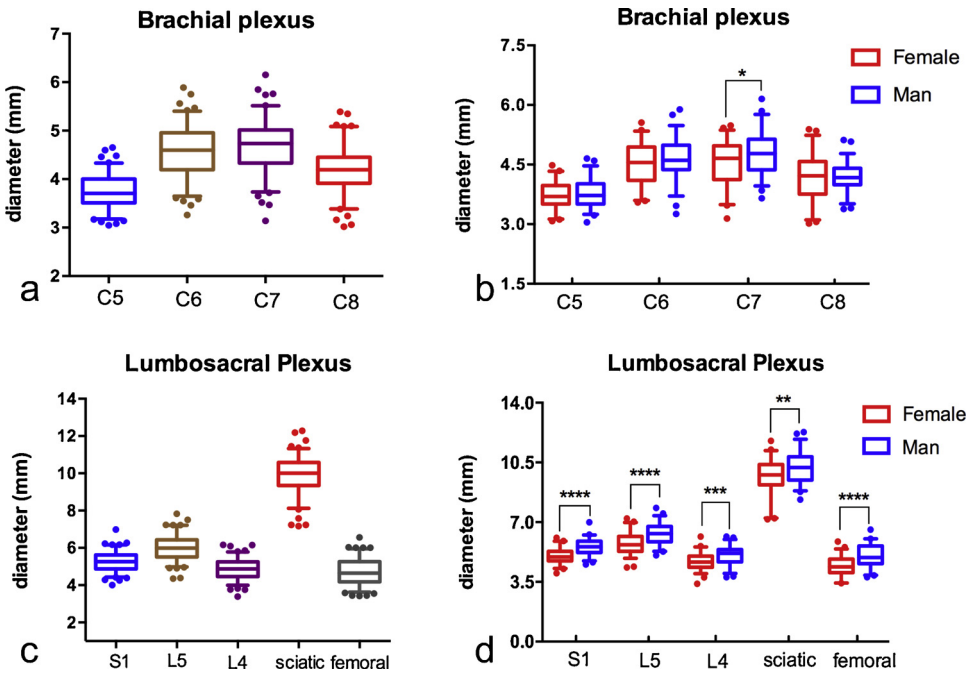

Fig. 3. There were significant differences in diameters between the individual nerve groups, except for between the L4 and femoral nerve roots (a, c). The diameters of the C7 (b) and L4-S1 nerve roots, and the sciatic and femoral nerves (d) were significantly larger in men than in women. There were no significant differences between the genders in the rest of the brachial plexus (b). *$P <$ 0.05, **$P <$ 0.001, ***$P <$ 0.0001, ****$P <$ 0.00001.

Table 3
Brachial and LS plexi CR and nT2 (Samples paired t test)[a].

	CR	*P* value	nT2	*P* value
BP	1.059 ± 0.05	0.475	3.07 ± 0.60	0.963
LSP	1.078 ± 0.05	0.061	—	0.000 *

CR: contrast ratio; nT2: T2 nerve-muscle signal ratio; BP: brachial plexus.

plexi were significantly lower than those of the corresponding nerve roots, but the ADC values were significantly higher (Table 4, all $P <$ 0.001).

3.8. Interreader and intrareader reliability

Good interreader reliability and intrareader reliability were obtained (intraclass correlation coefficients range from 0.703 to 0.996; Table 5).

4. Discussion

We presented the results of a comprehensive evaluation of the complex structure of the brachial and the LS plexi in the healthy adults, including the diameter of the macroscopic anatomy, the semi-quantitative T2 signal, the contrast enhancement, and the quantitative microstructure properties of the nerve root and ganglion. In addition, for quantitative normal reference ranges, we reported differences in terms of the left and right sides, the individual nerve groups, genders and ages differences.

In our study, no significant differences in parameters between the left and right sides were found. The finding supports the clinical practice of diagnosing neuropathies by comparing the nerves of interest with the contralateral side [16].

This study confirmed that men have larger nerve roots than women in the LS plexus and in parts of the brachial plexus. This is in accordance with the relationship between genders and the cross-sectional areas of the nerve trunks as seen on ultrasounds reported in the previous literature [17,18].

This study found no correlation between the nerve diameter and BMI. Currently there is no consensus on the possibility of a correlation between the nerve size and BMI. Peeters et al. reported a correlation between the cross-sectional areas of the ulnar nerve and BMI [19]. However, other related studies have found no correlation between the nerve size and BMI or body weight [20,21].

In the normal nerve tissues, the T2 relaxation time of the nerves is mainly organized into myelin, axonal, and extra-axonal water protons [22]. The axonal degeneration, especially the nerve edema due to the inflammatory changes, increases T2 relaxation time as shown by Hiwatashi et al., who demonstrated that patients with chronic inflammatory demyelinating polyneuropathy (CIDP) have longer T2 relaxation time than the healthy controls [10]. Therefore, it is important to recognize the normal profiles of the nT2 values in the nerve roots in

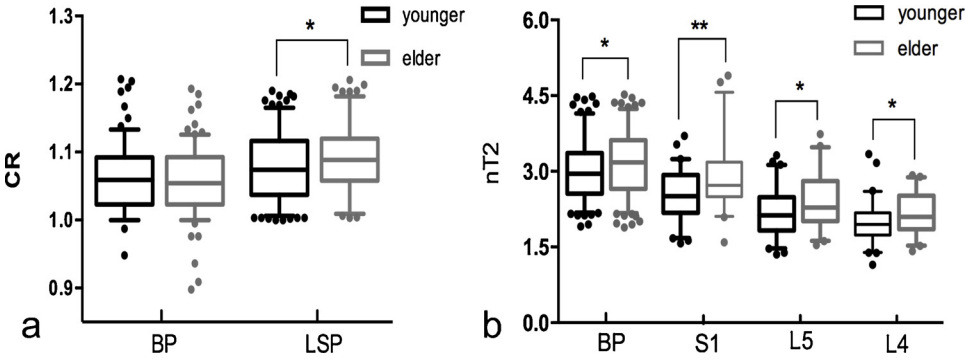

Fig. 4. The contrast ratio at the lumbosacral plexus nerve roots was significantly higher in the elder group than in the young group although there were no significant differences in the nerve roots of the brachial plexus (a). The T2 nerve-muscle signal ratio at the brachial, L4, L5, and S1 nerve roots were significantly higher in the elderly subjects (b). *$P <$ 0.05, **$P <$ 0.001.

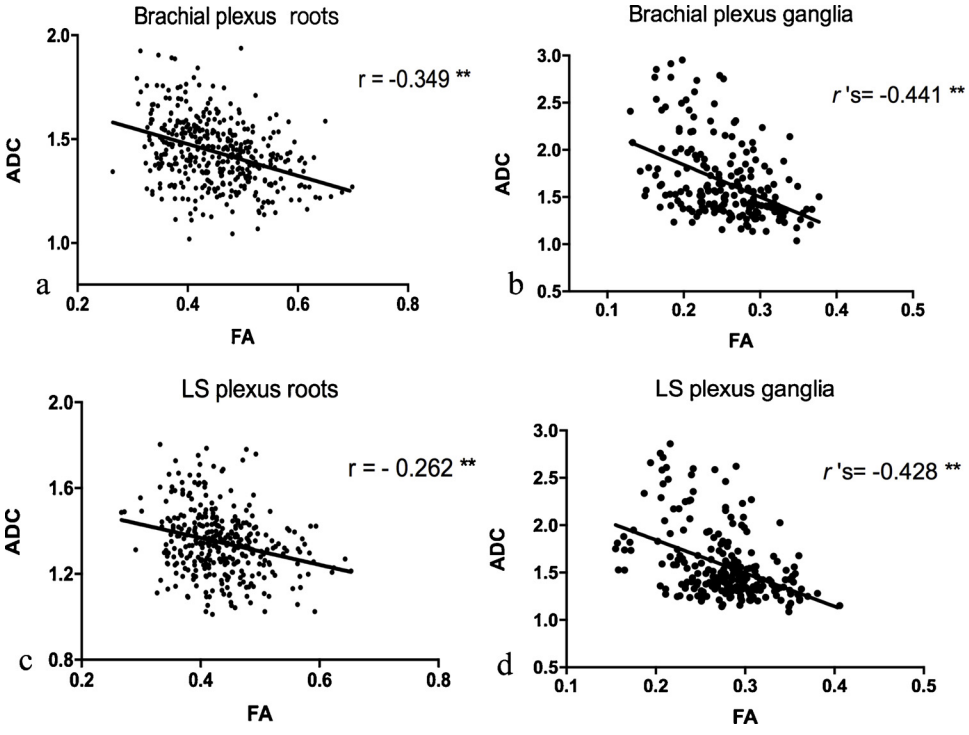

Fig. 5. A significant weak negative correlation was observed between the fractional anisotropy (FA) values and the apparent diffusion coefficients (ADC) at the nerve roots of the brachial (a, $r = -0.349$) and lumbosacral (LS) plexi (c, $r = -0.262$). Spearman rank correlation analysis showed a moderate negative correlation between the FA and ADC values at the ganglia of the brachial (b, r's $= -0.441$) and LS plexi (d, r's $= -0.428$). $^{**}P < 0.001$.

Table 4
Nerve roots and ganglia FA and ADC values (Wilcoxon signed-rank test)[a].

	FA (roots)	FA (ganglia)	*P* value	ADC (roots)	ADC (ganglia)	*P* value
C6	0.449 ± 0.07	0.240 (0.210, 0.288)	0.000	1.433 ± 0.15	1.570 (1.378, 1.968)	0.000
C7	0.479 ± 0.08	0.267 (0.235, 0.294)	0.000	1.400 ± 0.13	1.492 (1.370, 1.731)	0.000
S1	0.429 ± 0.07	0.278 (0.238, 0.299)	0.000	1.400 ± 0.16	1.480 (1.308, 1.678)	0.000
L5	0.429 ± 0.06	0.285 (0.251,0.316)	0.000	1.316 ± 0.15	1.420 (1.308, 1.678)	0.000

FA: fractional anisotropy; ADC: apparent diffusion coefficient; quartiles in parentheses;

order to detect any subtle changes. In this study we used the nT2 for the nerve assessment, a parameter that is used clinically and in the literature [23,24]. We found that the nT2 values were homogeneous in the brachial plexus, but increased from the top to the bottom in the LS plexus. These variances may be related to the structure of the LS plexus, since the L4-S1 nerves are more parallel to the long axis of the body. There may be more extra-axonal water protons at the bottom because of gravity, but this hypothesis needs further investigation.

In this study the nT2 and the CR values in the LS plexus significantly increased with the age increase while the S1 nerve root diameter decreased correspondingly. Additionally, a weak negative correlation between ages and the FA was observed. This finding could be attributed to the neurodegeneration and the continuous loss of nerve fibers, which also confirms the results of previously reported studies [21,25].

DTI has been recently applied in evaluating the different nerves in the upper and lower extremities, such as the median and peroneal nerves [11]. However, echo–planar-imaging-based DTI is susceptible to the motion artifacts and the geometric distortion, especially in the brachial plexus, which is more easily affected by the respiratory and pulsatile motions [13]. There are two methods for measuring the DTI parameters. One is to track fibers and average the values measured on multiple consecutive slices. However, this method cannot reflect the exact focal values. The other is to directly measure the focus of interest. However, the values generated are easily influenced by the adjacent isotropic cerebrospinal fluid [26]. Therefore, we set the three small ROIs over the same nerve root and then took an average.

The FA represents the proportion of the anisotropic components of the water molecules, while the ADC reflects the diffusion capacity. It has been demonstrated that there is a negative correlation between the FA and the ADC [27]. Furthermore, a significant increase in the ADC and a decrease in the FA were observed when the nerves were damaged due to changes in the directions and in the capacity of water molecule diffusion, which indicated the altered tissue integrity [27,28]. In our study, the FA values of the nerve roots were significantly higher than those of the corresponding ganglia, while the ADC values were lower. This difference may be due to the different anatomical structures of the ganglia and the nerve roots with the sensory cell bodies in the former and the sensory and motor nerve fibers in the latter.

Table 5
Interreader and Intrareader consistency (ICC correlation)[a].

	diameter (mm)(BP/LSP)	CR(BP/LSP)	nT2 (BP/LSP)	FA(BP/LSP)	ADC (BP/LSP)
Interreader	0.946/ 0.994	0.994/ 0.996	0.879/ 0.951	0.817/ 0.855	0.735/ 0.903
Intrareader	0.895/ 0.990	0.988/ 0.992	0.703/ 0.929	0.836/ 0.889	0.846/ 0.895

ICC: intraclass correlation coefficients; CR: contrast ratio; nT2: T2 nerve-muscle signal ratio; FA; fractional anisotropy; ADC: apparent diffusion coefficient; BP: brachial plexus; LSP: lumbosacral plexus.

In contrast to the perineurium and the endoneurial vessels of the nerve trunk, the DRG are permeable to low- and/or high-molecular-weight contrast agents under normal physiologic conditions [29,30]. In our study, the DRG showed avid enhancement. Diffuse or focal enhancements of the nerve roots can also be seen in immune-mediated inflammatory or entrapment disorders caused by the pathophysiological processes which increase the blood-nerve barrier permeability during demyelination and axonal degeneration. Therefore, the researchers should know when the increased enhancements and the CR values are normal or abnormal. Abnormal enhancements in the spinal roots, plexi, and cauda equina have been seen in patients with the Guillain–Barre´syndrome and CIDP [31,32]. Several studies have suggested that enhancements of the nerve roots may indicate disease activity [33,34]. The acquired normal contrast ratio of the plexi nerve roots using contrast agents in this study could be used for the inflammatory polyneuropathy in further studies. As the first to study the hemodynamic of the human sciatic nerve using dynamic contrast-enhanced (DCE) MR imaging, to my knowledge, Baumer et al. [35] provided the nerve blood volume and the blood-nerve permeability reference values that approximate the values of the white matter of the central nervous system. However, it is difficult to apply the DCE MR imaging to the plexus, because the nerve root volume is small and limited by poor signal noise ratio when using multi-phase dynamic scanning. Several studies have proposed to use sonography to assess the nerve perfusion. However, ultrasonography can only be applied to the superficial nerves instead of the deeper nerves which are usually affected by polyneuropathies [35,36].

The high interclass correlation coefficients indicate an excellent reproducibility of these measurements, which make them reliable to be used as normal references.

5. Limitations

First, our study was conducted at a single-center, and all the subjects were from the same ethnic group. Therefore, our study did not take into account the possible differences in the nerve parameters between different ethnic groups. Second, the brachial plexus group examination was performed on a 1.5-T MR scanner, while the LS and DTI groups examinations were performed on 3-T. The reason is that uniform fat suppression is more challenging to reach at 3-T, particularly in the neck region [37,38] than at 1.5-T. However, the brachial and LS plexi had completely independent parameters, were evaluated separately, and were not compared to each other. Third, we did not obtain permeability or T2 relaxation characteristics in plexi. Hopefully, improvements in hardware and MR techniques will be allowed for more advanced capabilities in tissue characterization. Fourth, we did not study the neuropathic diseases.

6. Conclusion

We have provided reference values for multimodal MR neurography, including the nerve diameter, CR, nT2, and DTI-based FA and ADC values. Parameter variations between the two sides, the individual nerves groups, genders, and the age groups were also discussed. These reference values have the potential to assist clinicians in detecting the subtle abnormalities possibly due to the neuropathic changes.

Conflicts of interest

The authors have no conflicts of interest to declare.

Acknowledgments

This work was supported by the National Natural Science Foundation of China (Grant No.81271570).

Appendix A. Supplementary data

Supplementary material related to this article can be found, in the online version, at doi:https://doi.org/10.1016/j.ejrad.2019.05.017.

References

[1] A. Tagliafico, G. Succio, G. Serafini, C. Martinoli, Diagnostic accuracy of MRI in adults with suspect brachial plexus lesions: a multicentre retrospective study with surgical findings and clinical follow-up as reference standard, Eur. J. Radiol. 81 (10) (2012) 2666–2672.
[2] M. Viallon, M.I. Vargas, H. Jlassi, K.O. Lovblad, J. Delavelle, High-resolution and functional magnetic resonance imaging of the brachial plexus using an isotropic 3D T2 STIR (short term inversion recovery) SPACE sequence and diffusion tensor imaging, Eur. Radiol. 18 (5) (2008) 1018–1023.
[3] K. Shibuya, A. Sugiyama, S. Ito, S. Misawa, Y. Sekiguchi, S. Mitsuma, Y. Iwai, K. Watanabe, H. Shimada, H. Kawaguchi, T. Suhara, H. Yokota, H. Matsumoto, S. Kuwabara, Reconstruction magnetic resonance neurography in chronic inflammatory demyelinating polyneuropathy, Ann. Neurol. 77 (2) (2015) 333–337.
[4] P. Murtz, M. Kaschner, F. Traber, G.M. Kukuk, S.M. Budenbender, D. Skowasch, J. Gieseke, H.H. Schild, W.A. Willinek, Evaluation of dual-source parallel RF excitation for diffusion-weighted whole-body MR imaging with background body signal suppression at 3.0 T, Eur. J. Radiol. 81 (11) (2012) 3614–3623.
[5] L. Wang, Y. Niu, X. Kong, Q. Yu, X. Kong, Y. Lv, H. Shi, C. Li, W. Wu, B. Wang, D. Liu, The application of paramagnetic contrast-based T2 effect to 3D heavily T2W high-resolution MR imaging of the brachial plexus and its branches, Eur. J. Radiol. 85 (3) (2016) 578–584.
[6] C.D. Sinclair, M.A. Miranda, P. Cowley, J.M. Morrow, I. Davagnanam, H. Mehta, M.G. Hanna, M. Koltzenburg, M.M. Reilly, T.A. Yousry, J.S. Thornton, MRI shows increased sciatic nerve cross sectional area in inherited and inflammatory neuropathies, J. Neurol. Neurosurg. Psychiatry 82 (11) (2011) 1283–1286.
[7] T. Lichtenstein, A. Sprenger, K. Weiss, K. Slebocki, B. Cervantes, D. Karampinos, D. Maintz, G.R. Fink, T.D. Henning, H.C. Lehmann, MRI biomarkers of proximal nerve injury in CIDP, Ann. Clin. Transl. Neurol. 5 (1) (2018) 19–28.
[8] T. Takagi, M. Nakamura, M. Yamada, K. Hikishima, S. Momoshima, K. Fujiyoshi, S. Shibata, H.J. Okano, Y. Toyama, H. Okano, Visualization of peripheral nerve degeneration and regeneration: monitoring with diffusion tensor tractography, Neuroimage 44 (3) (2009) 884–892.
[9] E.A. Neufeld, P.Y. Shen, A.E. Nidecker, G. Runner, C. Bateni, G. Tse, C. Chin, MR imaging of the lumbosacral plexus: a review of techniques and pathologies, J. Neuroimaging 25 (5) (2015) 691–703.
[10] A. Hiwatashi, O. Togao, K. Yamashita, K. Kikuchi, D. Momosaka, H. Nakatake, R. Yamasaki, H. Ogata, M. Yoneyama, J.I. Kira, H. Honda, Simultaneous MR neurography and apparent T2 mapping in brachial plexus: evaluation of patients with chronic inflammatory demyelinating polyradiculoneuropathy, Magn. Reson. Imaging 55 (2019) 112–117.
[11] M. Kronlage, V. Schwehr, D. Schwarz, T. Godel, L. Uhlmann, S. Heiland, M. Bendszus, P. Baumer, Peripheral nerve diffusion tensor imaging (DTI): normal values and demographic determinants in a cohort of 60 healthy individuals, Eur. Radiol. 28 (5) (2018) 1801–1808.
[12] N. Sollmann, D. Weidlich, B. Cervantes, E. Klupp, C. Ganter, H. Kooijman, E.J. Rummeny, C. Zimmer, J.S. Kirschke, D.C. Karampinos, High isotropic resolution T2 mapping of the lumbosacral plexus with T2-prepared 3D Turbo spin echo, Clin. Neuroradiol. (2018).
[13] P.K. van der Jagt, P. Dik, M. Froeling, T.C. Kwee, R.A. Nievelstein, B. ten Haken, A. Leemans, Architectural configuration and microstructural properties of the sacral plexus: a diffusion tensor MRI and fiber tractography study, Neuroimage 62 (3) (2012) 1792–1799.
[14] A. Tagliafico, B. Bignotti, G. Tagliafico, C. Martinoli, Peripheral nerve MRI: precision and reproducibility of T2*-derived measurements at 3.0-T : a feasibility study, Skeletal Radiol. 44 (5) (2015) 679–686.
[15] G. Gambarota, T2 relaxometry of human median nerve, Semin Musculoskelet. Radiol. 13 (1) (2009) 24–28.
[16] A. Tagliafico, A. Cadoni, E. Fisci, B. Bignotti, L. Padua, C. Martinoli, Reliability of side-to-side ultrasound cross-sectional area measurements of lower extremity nerves in healthy subjects, Muscle Nerve 46 (5) (2012) 717–722.
[17] J. Boehm, E. Scheidl, D. Bereczki, T. Schelle, Z. Aranyi, High-resolution ultrasonography of peripheral nerves: measurements on 14 nerve segments in 56 healthy subjects and reliability assessments, Ultraschall Med. 35 (5) (2014) 459–467.
[18] E. Scheidl, J. Bohm, M. Simo, C. Rozsa, B. Bereznai, T. Kovacs, Z. Aranyi, Ultrasonography of MADSAM neuropathy: focal nerve enlargements at sites of existing and resolved conduction blocks, Neuromuscul. Disord. 22 (7) (2012) 627–631.
[19] E.Y. Peeters, K.H. Nieboer, M.M. Osteaux, Sonography of the normal ulnar nerve at guyon's canal and of the common peroneal nerve dorsal to the fibular head, J. Clin. Ultrasound 32 (8) (2004) 375–380.
[20] R.A. Werner, J.A. Jacobson, D.A. Jamadar, Influence of body mass index on median nerve function, carpal canal pressure, and cross-sectional area of the median nerve, Muscle Nerve 30 (4) (2004) 481–485.
[21] L. Bathala, P. Kumar, K. Kumar, A. Shaik, L.H. Visser, Normal values of median nerve cross-sectional area obtained by ultrasound along its course in the arm with electrophysiological correlations, in 100 Asian subjects, Muscle Nerve 49 (2) (2014) 284–286.
[22] X. Zhang, F. Zhang, L. Lu, H. Li, X. Wen, J. Shen, MR imaging and T2 measurements

in peripheral nerve repair with activation of Toll-like receptor 4 of neurotmesis, Eur. Radiol. 24 (5) (2014) 1145–1152.
[23] P. Baumer, T. Dombert, F. Staub, T. Kaestel, A.J. Bartsch, S. Heiland, M. Bendszus, M. Pham, Ulnar neuropathy at the elbow: MR neurography–nerve T2 signal increase and caliber, Radiology 260 (1) (2011) 199–206.
[24] G. Meyer Zu, S. Horste, J. Cordes, C. Pfaff, A.K. Mathys, M. Mausberg, M. Bendszus, H.P. Pham, B.C. Hartung, Kieseier, Predicting the response to intravenous immunoglobulins in an animal model of chronic neuritis, PLoS One 11 (10) (2016) e0164099.
[25] N. Kabakci, B. Gurses, Z. Firat, A. Bayram, A.M. Ulug, A. Kovanlikaya, I. Kovanlikaya, Diffusion tensor imaging and tractography of median nerve: normative diffusion values, AJR Am. J. Roentgenol. 189 (4) (2007) 923–927.
[26] R. Miyagi, T. Sakai, E. Yamabe, H. Yoshioka, Consecutive assessment of FA and ADC values of normal lumbar nerve roots from the junction of the dura mater, BMC Musculoskelet. Disord. 16 (2015) 156.
[27] L.H. Markvardsen, M. Vaeggemose, S. Ringgaard, H. Andersen, Diffusion tensor imaging can be used to detect lesions in peripheral nerves in patients with chronic inflammatory demyelinating polyneuropathy treated with subcutaneous immunoglobulin, Neuroradiology 58 (8) (2016) 745–752.
[28] A. Heckel, M. Weiler, A. Xia, M. Ruetters, M. Pham, M. Bendszus, S. Heiland, P. Baeumer, Peripheral nerve diffusion tensor imaging: assessment of axon and myelin sheath integrity, PLoS One 10 (6) (2015) e0130833.
[29] A. B, A study of the perineurial diffusion barrier of a peripheral ganglion, Acta Neuropathol. (1979) 139–144.
[30] J.M. Jacobs, R.M. Macfarlane, J.B. Cavanagh, Vascular leakage in the dorsal root ganglia of the rat, studied with horseradish peroxidase, J. Neurol. Sci. 29 (1) (1976) 95–107.
[31] J.M. Vallat, C. Sommer, L. Magy, Chronic inflammatory demyelinating polyradiculoneuropathy: diagnostic and therapeutic challenges for a treatable condition, Lancet Neurol. 9 (4) (2010) 402–412.
[32] J. Duarte, A.C. Martinez, F. Rodriguez, A. Mendoza, A.P. Sempere, L.E. Claveria, Hypertrophy of multiple cranial nerves and spinal roots in chronic inflammatory demyelinating neuropathy, J. Neurol. Neurosurg. Psychiatry 67 (5) (1999) 685–687.
[33] S. Kuwabara, M. Nakajima, S. Matsuda, T. Hattori, Magnetic resonance imaging at the demyelinative foci in chronic inflammatory demyelinating polyneuropathy, Neurology 48 (4) (1997) 874–877.
[34] A.J. Duggins, J.G. McLeod, J.D. Pollard, L. Davies, F. Yang, E.O. Thompson, J.R. Soper, Spinal root and plexus hypertrophy in chronic inflammatory demyelinating polyneuropathy, Brain 122 (1999) 1383–1390.
[35] P. Baumer, M. Reimann, C. Decker, A. Radbruch, M. Bendszus, S. Heiland, M. Pham, Peripheral nerve perfusion by dynamic contrast-enhanced magnetic resonance imaging: demonstration of feasibility, Invest. Radiol. 49 (8) (2014) 518–523.
[36] K.R. Volz, K.D. Evans, C.D. Kanner, J.A. Dickerson, Detection of intraneural median nerve microvascularity using contrast-enhanced sonography: a pilot study, J. Ultrasound Med. 35 (6) (2016) 1309–1316.
[37] P. Murtz, M. Kaschner, A. Lakghomi, J. Gieseke, W.A. Willinek, H.H. Schild, D. Thomas, Diffusion-weighted MR neurography of the brachial and lumbosacral plexus: 3.0 T versus 1.5 T imaging, Eur. J. Radiol. 84 (4) (2015) 696–702.
[38] P. Murtz, C. Krautmacher, F. Traber, J. Gieseke, H.H. Schild, W.A. Willinek, Diffusion-weighted whole-body MR imaging with background body signal suppression: a feasibility study at 3.0 Tesla, Eur. Radiol. 17 (12) (2007) 3031–3037.